Dynamic and Structural Scalings of the Complexation Between *p*DNA and *b*PEI in Semidilute and Low-Salt Solutions

Rui Deng,[1] Shu Diao,[1] Yanan Yue,[1] To Ngai,[1] Chi Wu,[1,2,3] Fan Jin[1]

[1] *Department of Chemistry, The Chinese University of Hong Kong, Shatin, N.T., Hong Kong*

[2] *The Hefei National Laboratory of Physical Science at Microscale, The University of Science and Technology of China, Hefei, Anhui 230026, China*

[3] *Department of Chemical Physics, The University of Science and Technology of China, Hefei, Anhui 230026, China*

Received 21 September 2009; revised 7 January 2010; accepted 14 January 2010
Published online 1 February 2010 in Wiley InterScience (www.interscience.wiley.com). DOI 10.1002/bip.21399

ABSTRACT:

Using a combination of static and dynamic laser light scattering, we investigated the complexation of a supercoiled plasmid DNA (pDNA, 10^4 bp) and a branched polyethyleneimine (bPEI, M_w = 25 kD) in semidilute and low-salt aqueous solutions. Our results unearth some scaling laws for dynamic and structural properties of the resultant complexes (polyplexes) with different bPEI:pDNA (N:P) molar ratios. Namely, the average scattering intensity ($\langle I \rangle$) and the average linewidth of the Rayleigh peak ($\langle \Gamma \rangle$) are scaled to the scattering vector (q) as $\langle I \rangle \propto q^{\alpha_S}$ or $\langle \Gamma \rangle \propto q^{\alpha_D}$, where α_S and α_D are two N:P dependent scaling exponents. The N:P ratio strongly affects the complexation. When N:P < 2.0, the motions of the negatively charged and extended pDNA chains and the polyplexes are highly correlated so that they behave like a transient network with a fractal dimension. As the N:P ratio increases, nearly all of pDNA chains condensed and the overall charge of the polyplexes reverses to slightly positive, resulting in a turbid dispersion of large loose aggregates made of smaller, but more compact, polyplexes. Further increase of N:P finally disrupts large loose aggregates, leading to a homogeneous transparent dispersion of the polyplexes. © *2010 Wiley Periodicals, Inc. Biopolymers 93: 571–577, 2010.*

Keywords: conjugates of biostructures; gene delivery; laser light scattering

This article was originally published online as an accepted preprint. The "Published Online" date corresponds to the preprint version. You can request a copy of the preprint by emailing the Biopolymers editorial office at biopolymers@wiley.com

INTRODUCTION

Polyethyleneimine (PEI) has exhibited as a potential nonviral vector for gene delivery.[1,2] The positively charged PEI chains can condense the negatively charged plasmid DNA (*p*DNA) to form some compact DNA/PEI complexes, or called polyplexes.[3,4] Furthermore, not only such formed polyplexes can effectively enter cells via endocytosis but also successfully escape from endo-lysosomes to cytoplasm and then to nuclear because the protonization of PEI produces a "proton sponge" effect when they move from the extracellular space to the intercellular space.[5,6] The high in vitro transfection efficiency distinguishes the PEI-mediate nonviral vectors over others so that PEI is often used as a comparative standard.[1,4,5,7] The formation of the polyplexes is only the first step for the development of a good nonviral vector for gene delivery. Previous experimental results have indicated that many factors, such

Correspondence to: Fan Jin; e-mail: pizzball@gmail.com
Contract grant sponsor: National Natural Scientific Foundation of China (NNSFC)
Contract grant numbers: 20534020, 20574065
Contract grant sponsor: Hong Kong Special Administration Region (HKSAR)
Contract grant numbers: CUHK4037/06P, 2160298, CUHK402506, 2160291

as the ζ-potential, size, and density of the polyplexes, affect the final transfection efficiency.[8–10] In spite of thousands of publications, some of previous results are inconsistent, and even controversial. Therefore, it is necessary to revisit this complicated problem and understand the process in the microscopic level. Laser light scattering (LLS) and the ζ-potential analysis are two most convenient and useful methods for the characterization of the particle size, mass, and average surface potential.

Pecora et al.[11,12] and Cametti et al.[13,14] have used LLS to characterize DNA and polyplexes in dilute salted aqueous solutions. Note that in previous studies, the added salt screens strong electrostatic interaction so that the measurements became relatively simple. In real biological experiments, we sometimes have to use a semidilute or even concentrated low-salted solution. For instance, long *p*DNA ($>10^4$ bp) used to express more biofunctional proteins often has a supercoiled conformation, like a negatively charged rigid rod.[15] In this way, long and extended *p*DNA chains overlap with each other even though its concentration looks fairly low. This is because its overlap concentration (C^*) is related to the rod's length (L) and molar mass (M) as $C^*L^3 \cong M/N_A$, where, N_A is the Avogadro constant. Typically, $C^* \approx 1$ μg/mL for a 10^4-bp *p*DNA. It has been overlooked that the *p*DNA concentration normally used in the formation of polyplexes is already higher than C^*; that is, the solution is in the semidilute regime. Moreover, a low-salt condition sometimes is recognized to keep *p*DNA and the ploxplexes stable,[8,10] in which long range electrostatic interaction among the *p*DNA chains or polyplexes are expected. It has been shown that besides the first-order electrostatic repulsion, one has to consider the second-order electrostatic attraction. The like-charge attraction causes the coupled fluctuation of these binding counterions.[16] The chain overlapping and long-range electrostatic interaction make the characterization of the polyplexes extremely complicated and difficult.

In the current study, we tried to quantitatively study the condensation of a supercoiled *p*DNA (10^4 bp) with a branched PEI (*b*PEI, $M_w = 25$ kD) in semidilute and low-salt solutions using a combination of the ζ-potential and LLS measurements. The solution mixtures studied can be directly used to do in vitro gene transfection. We found that some of the solution mixtures have more than one relaxation mode and the relaxation is not purely diffusive. Our results reveal the existence of some scalings relationships between dynamic and structural properties of the polyplexes and the scattering vector (q) (or the observation length scale, $1/q$). Therefore, this study clearly demonstrated that the validity of those previous single-angle LLS characterizations of the polyplexes for gene transfection has to be considered.

MATERIALS AND METHODS

A *b*PEI ($M_w = 25$ kD, from Aldrich) was used without further purification. It is soluble in deionized water (18.2 MΩ · cm). Our LLS characterization shows that it has a broad molar mass distribution with an average molar mass of $\sim 2.5 \times 10^4$ g/mol, consistent with its specification. The plasmid, (pLUNIG-LIGL 10^4 bp), a lentivirus vector encoding both luciferase and enhanced green fluorescence protein, was prepared in our laboratory. The purification procedure was found elsewhere.[17] The gel electrophoresis (1% agarose in the TPEE buffer) shows two clear bands. The weaker and slower one is related to relaxed circular *p*DNA chains, while the stronger and faster one is attributed to supercoiled *p*DNA chains. The concentration of purified *p*DNA/Tris-EDTA solution determined by the UV absorption at 260 nm is 2 μg/μL. This concentrated *p*DNA solution was diluted to 20 μg/mL by dust-free deionized water passed through a 0.45 μm filter. The small volume (ca. 10 μL) of dust-free *b*PEI aqueous solution ($C = 3 \times 10^{-4}$ g/mL) was gently added stepwise to the 1.0 mL *p*DNA solution for the polyplexes formation at desired N:P ratios. The low-salt solution has a conductivity lower than 25 μS/cm, and the Debye-Hückel screening length is $\sim$ 2nm, which is much smaller than the presumed size of 10 kbp supercoiled *p*DNA and the $1/q$ spacings examined.

A commercial LLS instrument (ALV5000) with a vertically polarized 22 mW He-Ne laser head (632.8 nm, Uniphase) was used to investigate the process of the polyplexes formation. In dynamic LLS, the intensity–intensity time correlation function ($G^{(2)}(\tau)$) of the solution mixtures of *p*DNA and *b*PEI with different N:P ratios (0–16) was measured at different scattering angles (20–155°). $G^{(2)}(\tau)$ with two relaxation modes was analyzed by using the CONTIN[18] Laplace inversion program as well as the double-exponential fitting as follows,[18,19]

$$\{[G^{(2)}(\tau) - B]/B\}^{1/2} = A_{\text{fast}}(q)e^{-<\Gamma_{\text{fast}}>\tau} + A_{\text{slow}}(q)e^{-<\Gamma_{\text{slow}}>\tau}.$$

where B is the measured baseline, $<\Gamma>$ is the average characteristic linewidth of the Rayleigh peak, $A(q)$ is the intensity contribution of each relaxation mode, ($q \equiv (4\pi n/\lambda_0)\sin(\theta/2)$)) is the scattering vector with λ_0, n, and θ, the incident laser wavelength, the solvent refractive index, and the scattering angle. Note that $A_{\text{fast}}(q) + A_{\text{slow}}(q) \equiv 1$. The time-averaged scattering intensity from each mode can be calculated from the total time-averaged scattering intensity ($<I(q)>$) measured in static LLS and $A(q)$ from dynamic LLS, that is, $<I(q)>_{\text{fast}} = <I(q)>A_{\text{fast}}(q)$ and $<I(q)>_{\text{slow}} = <I(q)>A_{\text{slow}}(q)$.

The ζ-potential of the polyplexes was measured by a commercial Brookhaven Zeta Plus spectrometer with two platinum-coated electrodes and one He-Ne laser as the light source. Each mobility data point was averaged over 20 times that leads to the ζ-potential ($\zeta_{\text{Potential}}$) in the Hückel limit.[20]

RESULTS AND DISCUSSION

Figure 1a shows the typical measured intensity–intensity time correlation function for the complex formed at N:P of 1.5. The corresponding q-dependence of the intensity-weighted relaxation time distribution is depicted in Figure 1b. At low q value, there was only one relaxation mode while two distinct relaxation modes were observed at the high q value. Note that two relaxation modes are often found in the

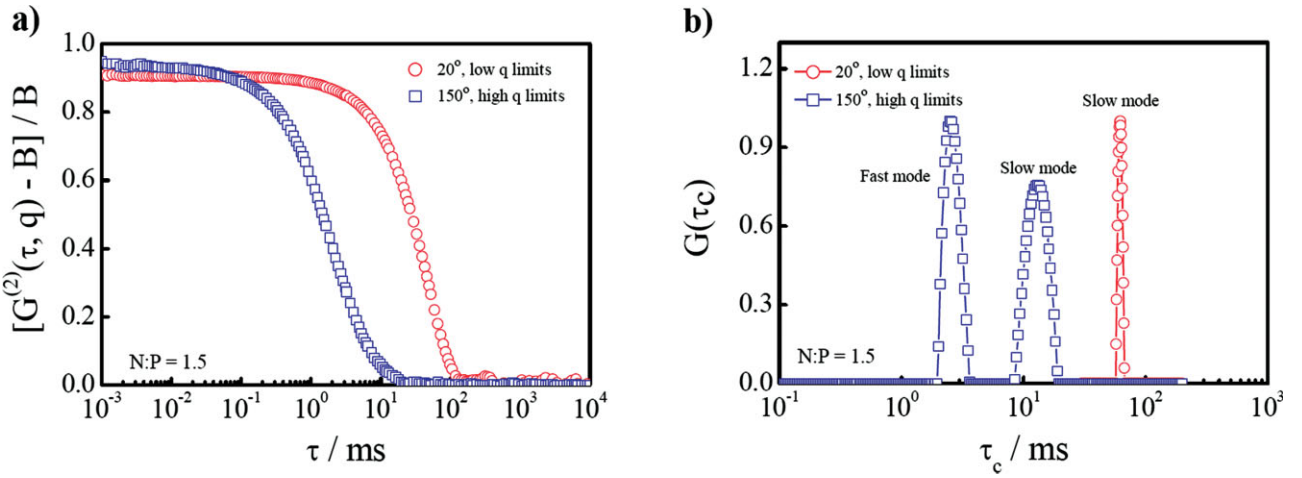

FIGURE 1 (a) Intensity correlation function at N:P = 1.5 with low q limits and high q limits, respectively; (b) corresponding relaxation time distribution from CONTIN fit.

dilute polyelectrolyte aqueous solution, particularly at low salt concentration, and the slow mode is usually much longer (1–2 orders) than the fast diffusive relaxation.[21,22] However, there is no clear interpretation for the origin of such slow mode. In most reported literatures, this slow relaxation was attributed to the long-ranged electrostatic interaction, but the theoretical calculation suggested that such a slow mode could only derive from the long-ranged attraction.[23–25] It is worthwhile to mention that the two modes observed in the present study were definitely different from those found in the dilute polyelectrolyte solution. First, it is the slow relaxation mode rather than the fast one that could be attributed to the diffusive relaxation. Second, no very slow relaxation mode was found in our system. One of the reasons may be due to the self-screening of highly negative-charged supercoiled DNA in the semidilute state. Presumably, if there has very slow relaxation mode in our system, it cannot fully relax to zero within the delay time window of a few seconds.

Figure 1b clearly shows that the two peaks were well separated and narrowly distributed indicating that the slow and fast relaxations were fully decoupled in the Fourier space and the error in the inverse Laplace transform was limited. Therefore, the pure slow motion could be extracted from the measured time correlation function without affecting the fast mode. The plot of $<\Gamma_{slow}>$ vs. q^2 (data not shown) had a nonliner relation; revealing that it is not a purely diffusive. Thus, a double logarithmic plot was used in the present study to explore the nature of relaxation mode.

Figure 2 shows the scattering vector (q) dependence of the average linewidths of two relaxation modes ($<\Gamma_{fast}>$ and $<\Gamma_{slow}>$) in the *p*DNA solution after the addition of different amounts of *b*PEI. $<\Gamma>$ can be scaled to q as $<\Gamma> \propto q^{\alpha_D}$, where α_D is a dynamic scaling exponent and the slope of each fitting line in Figure 2. Depend on the *b*PEI concentration, the q-dependant of $<\Gamma>$ shows that the complexation has three different stages. Namely, the solution mixture is stable with two relaxation modes ($<\Gamma_{fast}>$ and $<\Gamma_{slow}>$) when $0 \leq$ N:P $\leq$ 1.5. The increase of N:P to the range 2.0–6.0 results in an unstable solution mixture with only one relaxation mode and different q-dependent scaling exponents α_D. Further addition of *b*PEI finally leads to a homogeneous dispersion with a purely diffusive relaxation mode ($\alpha_D = 2.0$) in the N:P range 8.0–16.0. It is worth noting that $<\Gamma_{fast}>$ is nearly independent of q in the pure *p*DNA solution (N:P = 0), suggesting an internal relaxation of rod-like rigid *p*DNA chains with a frequency of $\sim$ 1 kHz, consisting with some previous experimental results.[15] For the slow mode, $\alpha_D \approx 1.7$, indicating that the relaxation is not purely diffusive (random walk). Note that such a nonlinear Γ/q^2 relation was not caused by either polydispersity or internal motions, because the used *p*DNA was nearly monodisperse (from small angel DLS and gel electrophoresis data) and the effects of internal motions were minimized by CONTIN fitting. Moreover, the existence of polydispersity and internal motions would lead to $\alpha_D > 2$ with a $q \to 0$, $\Gamma \to 0$ limits. We thereby suggest that the small α_D obtained here is presumably because of the strong electrostatic interaction among different *p*DNA chains. Note that such a more "ordered" relaxation mode ($\alpha_D < 2.0$) has also been observed in some semidilute solutions and gels.[26] Therefore, previous single-angle LLS measurements of *p*DNA or polyplexes in such a complicated dispersion likely led to an incorrect hydrodynamic size.

Figure 3 shows the scattering vector (q) dependence of the average scattering intensity contributions $<I>$ from each relaxation mode at different N:P ratios. $<I>$ is also scaled to q as $<\Gamma> \propto q^{\alpha_D}$, where α_S is the static scaling exponent. There also exist three different stages similar to those in Fig-

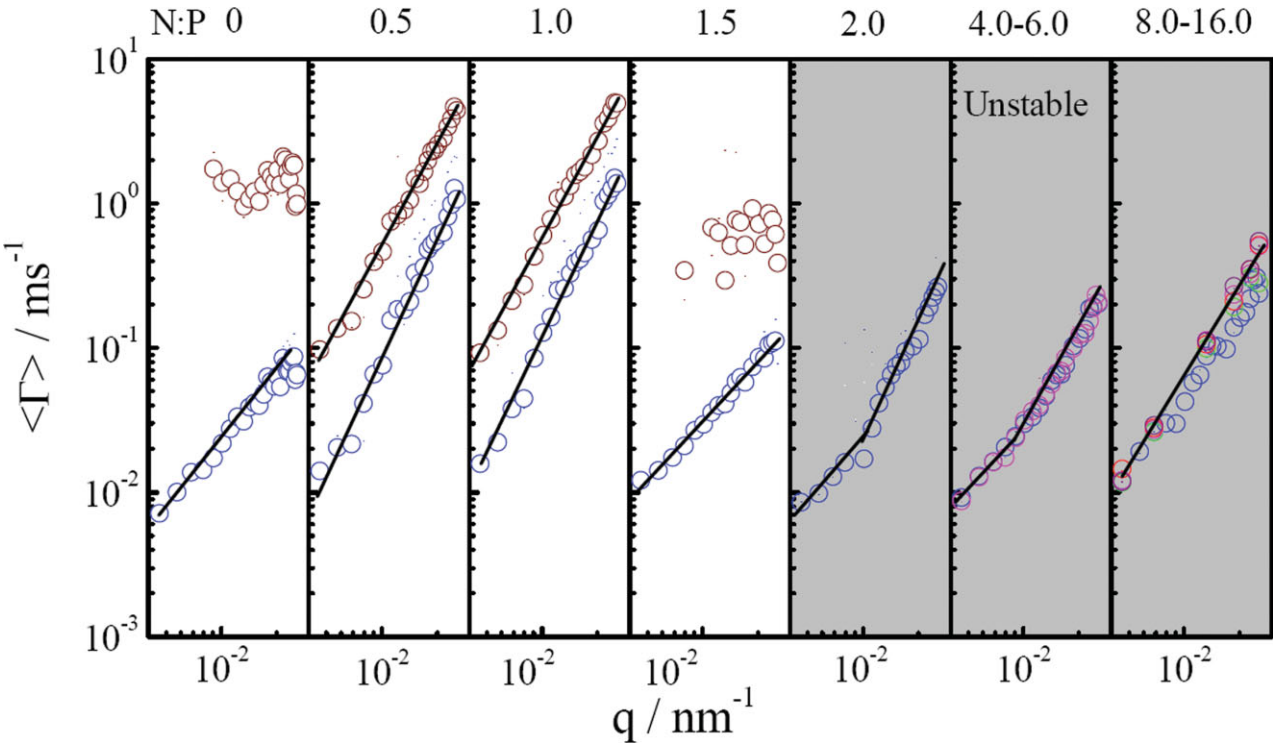

FIGURE 2 Scattering vector (q) dependence of average linewidths of two relaxation modes ($<\Gamma_{fast}>$and $<\Gamma_{slow}>$) with different N:P ratios (0–16) in low-salt aqueous solutions, where each line represents a fitting of $<I> \propto q^{-\alpha_s}$ and each slope leads to a dynamic scaling exponent (α_D). Different colors represent different N:P ratios when 4.0 < N:P < 16.0.

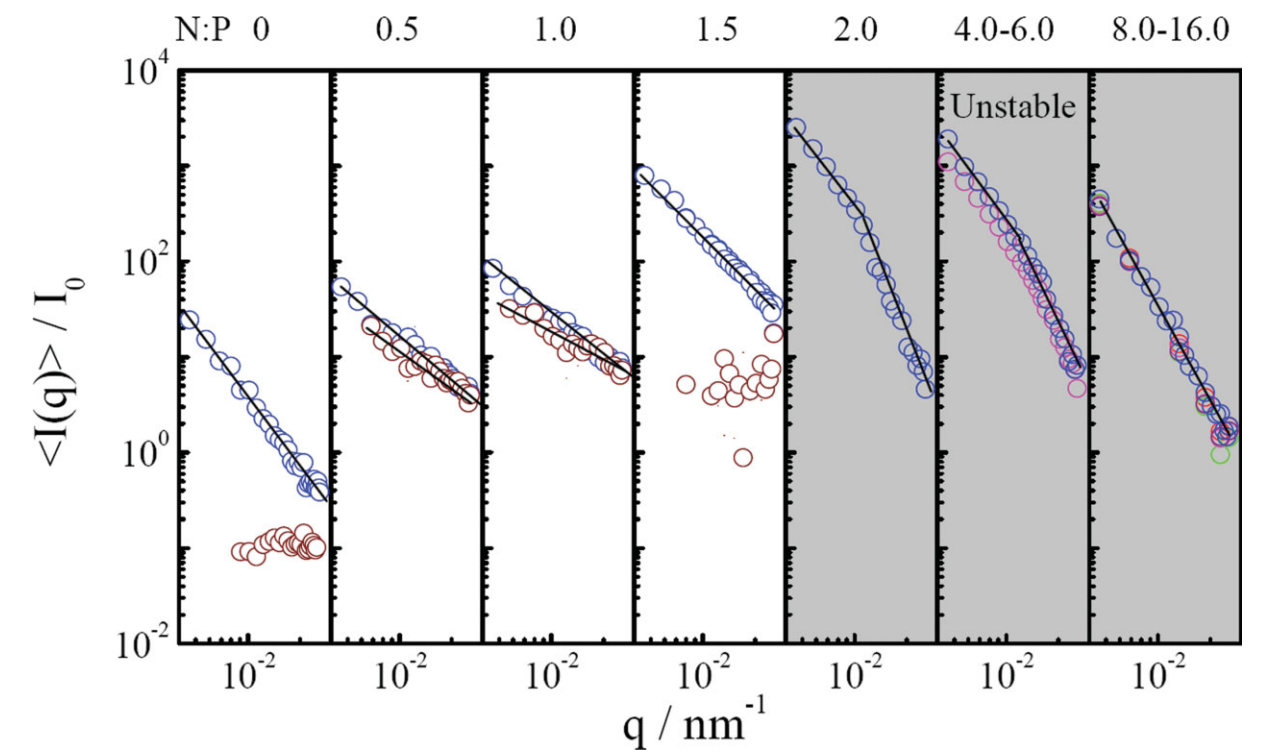

FIGURE 3 Scattering vector (q) dependence of average scattering intensities of corresponding to two relaxation modes ($<I_{fast}>$and $<I_{slow}>$) with different N:P ratios (0–16) in low-salt aqueous solutions, where each line represents a fitting of $<I> \propto q^{-\alpha_s}$ and each slope leads to a static scaling exponent (α_S). Different colors represent different N:P ratios when 4.0 < N:P < 16.0.

ure 2. When $0 \leq$ N:P ≤ 1.5, the observed static scaling relation suggests that the solution mixture behaves like a transient network with a fractal dimension in our observed length scale (30 nm $< q^{-1} <$ 300 nm). α_S reflects the fractal dimension of such a network. The higher α_S,the dimensional "denser" it is.[27] A combination of α_D and α_S leads to some insights of different stages as follows. In the first stage ($0 \leq$ N:P ≤ 1.5), when N:P $= 0$ in the pure *p*DNA solution, the extended supercoiled *p*DNA chains are overlapped with each others to form a transient network with a fractal dimension of $\alpha_S = 2.3$. In the N:P range 0.5–1.0, the added *b*PEI chains can only complex and condense a fraction of *p*DNA chains, making the transient network loose and leaving some "holes" inside. Presumably, the resultant polyplexes are embedded inside these holes and surrounded by the rest of loosely overlapped *p*DNA chains, leading to two relaxation modes; namely, $\alpha_S = 1.3$ for the loosely overlapped *p*DNA chains and $\alpha_S = 1.2$ for those embedded polyplexes. As expected, both of them have a lower fractal dimension. Further addition of *b*PEI (N:P $= 1.5$) condenses more *p*DNA, resulting in more polyplexes so that the *p*DNA transient network starts to "dissolve" into a dispersion of highly inter-connected polyplexes transient network. In the second stage ($2.0 \leq$ N:P $\leq$ 6.0), on the one hand, the *b*PEI chains condense nearly all the *p*DNA chains to form the *p*DNA/*b*PEI polyplexes; on the other hand, each *b*PEI chain can complex with more than one *p*DNA chain so that a number of individual compact polyplexes are loosely inter-connected to form a large aggregate. This is why we have different static scaling exponents in different q ranges. The dynamic slowing down and some correlation between these larger aggregates are expected because of long-ranged electrostatic interaction. In the third stage ($8.0 \leq$ N:P ≤ 16.0), the addition of excess *b*PEI chains finally disrupts those large aggregates made of loosely connected polyplexes to form individual compact polyplexes with a more uniform density. Note that the addition of *b*PEI increases the scattering intensity over $\sim$ 100 times, resulting in the polyplexes with a final average hydrodynamic radius of $\sim$ 500 nm. A simple calculation reveals that on average, each the resultant polyplex contains more than one *p*DNA chains. The existence of an excessive amount of *b*PEI chains free in the solution mixture completely screens any possible interaction among different polyplexes so that the relaxation becomes purely diffusive with $\alpha_D = 2.0$.

Figure 4 shows the N:P ratio dependence of the scaling exponents (α_S and α_D) and the ζ-potential of the solution mixtures. As expected, the average ζ-potential of an initial pure *p*DNA solution is negative. In the first stage, both α_S and α_D vary as a fraction number of *p*DNA chains, which are complexed with the *b*PEI chains added to form the *p*DNA/

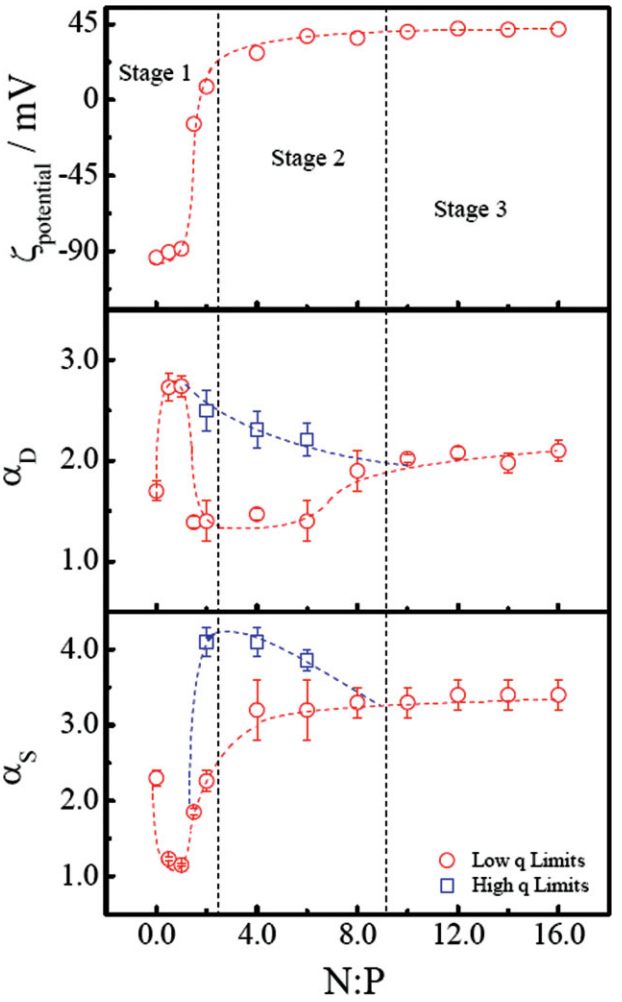

FIGURE 4 N:P ratio dependence of the static and dynamic scaling exponents (α_S and α_D) and average ζ-potential ($\zeta_{Potential}$) in low-salt aqueous solutions, where two dash lines divided the studied N:P range in three stages: (1) $0 \leq$ N:P ≤ 1.5; (2) $2.0 \leq$ N:P ≤ 6.0; (3) $8.0 \leq$ N:P ≤ 16.0.

*b*PEI polyplexes. The polyplexes are embedded inside the transient network made of the rest of loosely overlapped *p*DNA chains. In the second stage, the addition of positively charged *b*PEI inverses the average ζ-potential from negative to positive. Both α_S and α_D exhibit different behaviors in different observation length scales ($1/q$). In the low q limit, $\alpha_S = 2.3$ and $\alpha_D = 1.5$ reflecting that there exists a loose transient network-like structure with a relatively slower relaxation over the long observation length scale[28]; while in the high q limit $\alpha_S = 4.0$ and $\alpha_D = 2.5$, revealing individual localized compact polyplexes inside each large polyplex aggregate. Their diffusive relaxation is mixed with a faster internal motions.[27] Note that the crossover occurs at $q^{-1} \approx$ 100 nm, presumably corresponding to the static correlation size of individual polyplexes. Finally, in the third stage, α_S

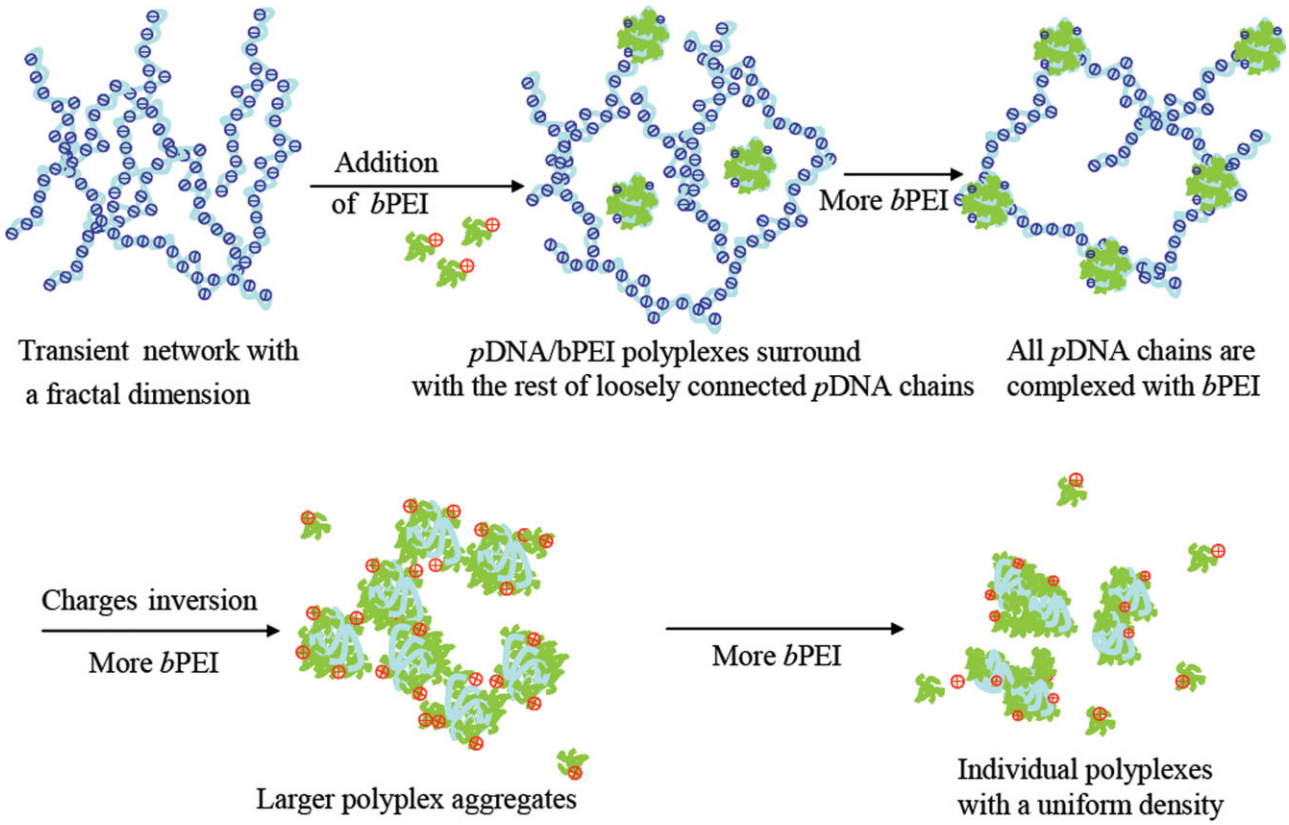

FIGURE 5 Schematic of complexation between *p*DNA and *b*PE in a semidilute low-salt aqueous solution, where blue helixes and green stars respectively represent supercoiled *p*DNA and branched *b*PEI chains. Negative and positive charges are symbolically labeled as "−" and "+", respectively.

approaches 3.0 over the entire q range, indicating that individual compact polyplexes has a uniform density. Figure 5 schematically summarizes earlier discussion; namely, the addition of *b*PEI weakens the transient *p*DNA network and leads to the formation of some embedded *p*DNA/*b*PEI polyplexes; more further addition of *b*PEI gradually "dissolves" the transient *p*DNA network and results in unstable polyplexes that flocculate with each other to form large aggregates with a loose structure; and finally, the excess amount of free *b*PEI chains disrupt large aggregates, leading to the formation of individual stable compact polyplexes with a uniform density.

CONCLUSIONS

Our current results about the complexation between anionic pLUNIG-LIGL plasmid (pDNA) and cationic *b*PEI in semidilute and low-salt aqueous solutions reveal that in a general preparation of the *p*DNA/*b*PEI polyplexes for gene transfection, long *p*DNA chains ($> 10^4$ bp) in the solution are overlapped with each other to form a transient network even before the addition of *b*PEI. In other words, the *p*DNA solution used in a gene transfection experiment is already semidilute even though its concentration is very low. This is because the negatively charged *p*DNA chains are extended and correlated due to long range electrostatic interaction. A gradual addition of cationic *b*PEI leads to different three complexation stages, depending on the N:P ratio. In the first stage, only a fraction number of *p*DNA chains are complexed with the added *b*PEI chains and the resultant *p*DNA/*b*PEI polyplexes are embedded inside a weakened transient network made of the rest of loosely overlapped *p*DNA chains. In the second stage, the addition of more *b*PEI gradually inverses the overall charge of the polyplexes from negative to positive and destabilizes the polyplexes so that they flocculate with each other to form large loosely connected aggregates. In the third stage, further addition of *b*PEI disrupts large polyplex aggregates into individual polyplexes with a uniform density. Previous studies have overlooked the complicated nature of the complexation of *p*DNA and *b*PEI in a solution mixture. The outcome of this study enables us to design and prepare better *p*DNA/*b*PEI polyplexes for in vitro gene transfection.

REFERENCES

1. Boussif, O.; Lezoualc'h, F.; Zanta, M. A.; Mergny, M. D.; Scherman, D.; Demeneix, B.; Behr, J. P. Proc Natl Acad Sci USA 1995, 92, 7297–7301.
2. Godbey, W. T.; Wu, K. K.; Mikos, A. G. J Control Release 1999, 60, 149–160.
3. Thomas, M.; Klibanov, A. M. Proc Natl Acad Sci USA 2002, 12, 14640–14645.
4. Pack, D. W.; Hoffman, A. S.; Pun, S.; Stayton, P. S. Nat Rev Drug Discov 2005, 4, 584–593.
5. Akinc, A.; Thomas, M.; Klibanov, A. M.; Langer, R. J Gene Med 2005, 7, 657–663.
6. Sonawane, N. D.; Szoka, F. C., Jr.; Verkman, A. S. J Biol Chem 2003, 278, 44826–44831.
7. Breunig, M.; Lungwitz, U.; Liebl, R.; Goepferich, A. Proc Natl Acad Sci USA 2007, 104, 14454–14459.
8. Wightman, L.; Kircheis, R.; Rossler, V.; Carotta, S.; Ruzicka, R.; Kursa, M.; Wagner, E. J Gene Med 2001, 3, 362–372.
9. Godbey, W. T.; Wu, K. K.; Mikos, A. G. J Biomed Mater Res Part A 1999, 45, 268–275.
10. Vijayanathan, V.; Thomas, T.; Shirahata, A.; Thomas, T. J Biochem 2001, 40, 13644–13651.
11. Sorlie, S. S.; Pecora, R. Macromolecules 1990, 23, 487–497.
12. Seils, J.; Pecora, R. Macromolecules 1992, 25, 354–362.
13. Marchetti, S.; Onori, G.; Cametti, C. J Phys Chem B 2005, 109, 3676–3680.
14. Marchetti, S.; Onori, G.; Cametti, C. J Phys Chem B 2006, 110, 24761–24765.
15. Seils, J.; Pecora, R. Macromolecules 1995, 28, 661–673.
16. Manning, G. Accounts Chem Res 1979, 12, 443–449.
17. Marko, M. A.; Chipperfield, R.; Birnboim, H. C. Anal Biochem 1982, 121, 382–387.
18. Berne, B.; Pecora, R. In Dynamic Light Scattering; Plenum Press: New York, 1976.
19. Chu, B. In Laser Light Scattering,2nd ed.; Academic Press: New York, 1991.
20. Hunter, R. J. In Foundations of Colloid Science, 2nd ed.; Oxford University Press: Oxford, 2000.
21. Lin, S. C.; Lee, W. I.; Schurr, J. M. Biopolymers 1978, 17, 1041–1066.
22. Schmitz, K. S.; Lu, M.; Gauntt, J. J Chem Phys 1983, 78, 5059–5066.
23. Dobrynina, A. V.; Rubinstein, M. Prog Polym Sci 2005, 30, 1049–1118.
24. Lee, W. I.; Schurr, J. M. Chem Phys Lett 1973, 23, 603–607.
25. Muthukumar, M. J. Adv Chem Phys 2005, 131, 1–23.
26. Li, J. F.; Li, W.; Huo, H.; Luo, S. Z.; Wu, C. Macromolecules 2008, 41, 901–911.
27. Mandlbrot, B. J. In Fractals, Form and Dimensions; Freeman: San Francisco, 1977.
28. Weitz, D. A.; Huang, J. S.; Lin, M. Y.; Sung, J. Phys Rev Lett 1985, 54, 1416–1419.

Reviewing Editor: Sarah Woodson